Airflow and Precipitation Structure of Two Leading Stratiform Mesoscale Convective Systems Determined from Operational Datasets

CRYSTALYNE R. PETTET* AND RICHARD H. JOHNSON

Atmospheric Science Department, Colorado State University, Fort Collins, Colorado

(Manuscript received 5 November 2002, in final form 15 April 2003)

ABSTRACT

An analysis of the airflow and precipitation structure of two leading stratiform (LS) mesoscale convective systems (MCSs) is presented. Leading stratiform systems are defined as linear MCSs that consist of a convective line with leading stratiform rain. Case studies of LS systems on 7 May 1997 and 30 April 2000 were conducted using the available operational datasets. Several of the features observed, though not all, appear as a mirror image of those seen in trailing stratiform (TS) mesoscale convective systems. Their horizontal reflectivity structure has similar aspects, with convective cells that are sometimes elongated and canted with respect to the convective line, a transition zone of lower reflectivity, and an area of enhanced stratiform rain. The 30 April case shows a leading mesolow that resembles a TS wake low, but its propagation characteristics (and presumably dynamics) differ. A descending leading inflow jet, the counterpart of a rear-inflow jet in a TS system, can be detected in both cases underneath a layer of strong ascending rear-to-front flow aloft.

A few features of these LS systems are distinctive from TS systems. Cells in the convective line appear to be more discontinuous, and are elongated more than those of a TS system, although more work is needed to quantify these distinctions. Rear-feeding from an elevated equivalent potential temperature maximum behind the system is a distinguishing feature of these LS MCSs, since TS MCSs are typically fed from the boundary layer. Unlike the rear-inflow jet in TS systems, neither case shows a reversal in the leading inflow jet as it descends to low levels near the convective line. Both cases exhibit front-to-rear storm-relative surface flow throughout the LS systems.

Finally, a conceptual model is presented that illustrates the structure observed in the two cases, based heavily on a single-Doppler radar analysis of 7 May 1997.

1. Introduction

A common pattern of organization of mesoscale convective systems (MCSs) is the leading-line/trailing stratiform structure (hereafter referred to as TS), first identified in tropical MCSs by Zipser (1969, 1977) and Houze (1977), and later in midlatitude MCSs by Smull and Houze (1985), Houze et al. (1989), and others. Using Weather Surveillance Radar-1988 Doppler (WSR-88D) data, Parker and Johnson (2000) identified two other modes of organization for linear MCSs: a convective line with leading stratiform rain (LS), and a convective line with parallel stratiform rain (PS). They found that while TS is the most common mode of organization, accounting for nearly 60% of the 88 cases studied, both LS and PS modes are not negligible, each accounting for nearly 20% of the total. While the spatial patterns of precipitation in these two modes have been identified, their internal circulation features have not been determined. As a first step in this direction, this study will focus on the LS mode of organization and diagnose the circulation features of LS MCSs by examining available operational datasets for two LS systems.

One motivation for exploring the circulation characteristics of LS MCSs stems in part from their potentially important role in flash floods. In Parker and Johnson (2000) it was found that of the three modes of organization, LS systems were the slowest, on average, with a number of cases having speeds of 5 m s^{-1} or less. As a consequence, some LS MCSs have been found to produce heavy rainfall. Of the LS systems, Parker and Johnson (2000) identified two types of low-level moist inflow: storm-relative inflow from the front (''front fed''), and from the rear (''rear fed''). Since rear-fed systems have the potential for ''back building'' and the repeated formation and movement of cells over the same location, a process implicated in flash floods (Chappell 1986; Doswell et al. 1996), this study will examine two LS MCSs, both of which exhibited rear-

* Current affiliation: Atmospheric Technology Division, National Center for Atmospheric Research, Boulder, Colorado.

Corresponding author address: Crystalyne R. Pettet, ATD/NCAR, P.O. Box 3000, Boulder, CO 80307.
E-mail: pettet@atd.ucar.edu

fed characteristics. However, only one of the two produced flash floods.

There has not been a field study dedicated to collecting data on LS MCSs, and therefore operational datasets are utilized in this study. It is recognized that two LS MCSs represent a sample too small to permit gross generalizations of results; however, this exploratory study will reveal a number of similar circulation features within rear-fed LS MCSs that are suggestive of common behavior of such systems. Further, this study will provide a foundation for further observational studies of these phenomena.

This paper is organized in the following manner: section 2 discusses the different datasets utilized for this study and the methods used to analyze them, section 3 provides case studies of two LS systems—one on 7 May 1997 and the other on 30 April 2000, and section 4 synthesizes the two cases and summarizes the findings of this study, along with study conclusions and providing plans for future research.

2. Data analysis

This study makes use of several operational datasets. National Oceanic and Atmospheric Administration (NOAA) Wind Profiler Network (NPN) data, Oklahoma Mesonet data (Brock et al. 1995), both single-site and national mosaic Next Generation Weather Radar (NEXRAD) WSR-88D data, 40- and 60-km Rapid Update Cycle (RUC) model analysis data[1] (Benjamin et al. 1998), National Weather Service rawinsonde soundings, National Centers for Environmental Prediction (NCEP) analysis charts, surface data, and satellite data were analyzed. Analysis methods for some of the datasets are described below.

NOAA Wind Profiler Network data were gridded to a 75 km × 75 km × 250 m grid using a Barnes (1973) filter. Vertical slices were taken perpendicular to the convective line of the MCS to analyze cross-line flow. A storm motion vector was subtracted from the profiler data to determine storm-relative flow. Divergence was calculated using centered finite differencing of the gridded data, which were then used to calculate vertical motion using the kinematic method with the O'Brien (1970) correction.

Oklahoma Mesonet data were gridded to a 10 km × 10 km grid using a Barnes objective analysis technique (Barnes 1973; Koch et al. 1983). Since mesonet sites vary in elevation, pressures were hydrostatically adjusted to an elevation of 366 m, the average elevation of all mesonet stations. Time-to-space conversions were also performed on the mesonet data (Fujita 1955; Pedgley 1962) assuming a steady-state storm motion over 30 min.

The WSR-88D level II radial velocity data were used to investigate the internal circulation features of the LS MCSs, and to examine their vertical structure. Radial velocities were used to determine the vertical structure of the flow normal to the main convective line as in Houze et al. (1989). Radial velocity folds were manually unfolded using the Research Data Support System (RDSS) software developed at the National Center for Atmospheric Research (NCAR; Oye and Carbone 1981). The data were gridded to a 1 km × 1 km × 0.5 km grid using a Cressman filter. Vertical cross sections were taken along the line of storm motion so that storm motion could be subtracted out, yielding storm-relative radial velocities along the cross section. Other cross sections were examined as well to further investigate the reflectivity structure, but storm-relative winds were not calculated for these because they would be ambiguous. Because the gridding process tends to smooth out some reflectivity features, cross sections of ungridded reflectivity were also analyzed in radial coordinates.

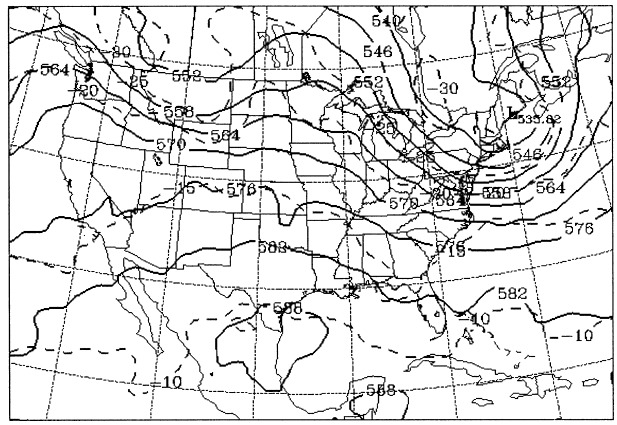

FIG. 1. The 500-hPa heights (dm, solid) and temperatures (°C, dashed) from the Eta Data Assimilation System (EDAS).

3. Case studies

Two cases having prominent LS precipitation structure and lifetimes greater than 6 h were selected for study, one on 7 May 1997 and the other on 30 April 2000. The 7 May 1997 case was identified as an LS MCS in Parker and Johnson (2000). Doppler radar data were available for this case, allowing radial velocities to be used to identify the internal circulation features of the storm.

The 30 April 2000 case was identified using real-time observations from the operational network while it was producing heavy rainfall and flooding in some areas. The storm spent a significant fraction of its lifetime over the Oklahoma Mesonet and the NOAA NPN. Although the storm was situated in the densest portion of the profiler network, these data cannot resolve its internal circulation features; rather, they provide a coarse depiction of the flow within the storm and its mesoscale environment. High-resolution Oklahoma Mesonet data

[1] Two versions are used because the RUC was updated in 1998.

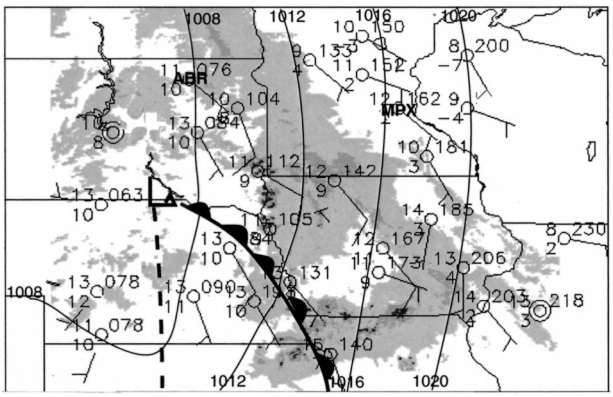

FIG. 2. Surface analysis for 1200 UTC on 7 May 1997. Radar reflectivity is shaded: light gray = 20–40 dBZ, dark gray = 40–50 dBZ, and black ≥ 50 dBZ. Pressure is contoured every 4 hPa. Sounding locations MPX and ABR are indicated.

provide information to examine the surface features of the LS system. Although the LS MCS passed directly over the Frederick, Oklahoma, Doppler radar site, the data were not archived, making them unavailable for this study.

a. LS MCS on 7 May 1997

On 7 May 1997 an MCS formed over South Dakota and moved across Minnesota and Iowa. The system moved rapidly (15 m s^{-1}), so it did not produce flooding. It did, however, pass directly over the Sioux Falls, South Dakota, WSR-88D radar, providing high-resolution Doppler radar data to analyze.

1) SYNOPTIC ENVIRONMENT

The upper-level flow pattern at 1200 UTC on 7 May 1997 was dominated by a ridge over the central United States (Fig. 1). A trough was located over New England, with another trough across Montana and Wyoming. At the surface, a low was located over south-central South Dakota (Fig. 2). A trough extended south from the low. A warm front extended from the low parallel to the Nebraska–South Dakota and Nebraska–Iowa borders. A significant stratiform rain area developed ahead (east) of a convective line along the Iowa–South Dakota border.

Soundings were taken behind (west of) and ahead (east of) of the MCS at 1200 UTC (see Fig. 2 for locations). The sounding ahead of the MCS at Chanhassen, Minnesota (MPX, Fig. 3a), shows a significant temperature inversion at the surface. Midlevel air was largely at or near saturation, but low-level air was fairly dry. A low-level southerly jet was located atop the inversion. The sounding behind the LS system at Aberdeen, South Dakota (ABR, Fig. 3b) shows nearly saturated conditions from 800 to 500 hPa. A strong capping inversion appears between 880 and 850 hPa. Surface parcels have no buoyancy in either sounding; therefore, convection was likely elevated. Both of these soundings indicate a southerly low-level wind that generally veers with height to southwesterly in the mid- to upper troposphere, suggestive of warm advection across this region. Another sounding taken at Omaha, Nebraska (OAX, not shown), had 18 m s^{-1} winds from 200° to 210° at 850–875 hPa. The warm advection indicated by these soundings likely contributed to upward vertical motion, which is also reflected by the development of elevated thunderstorms (e.g., Maddox and Doswell 1982; Colman

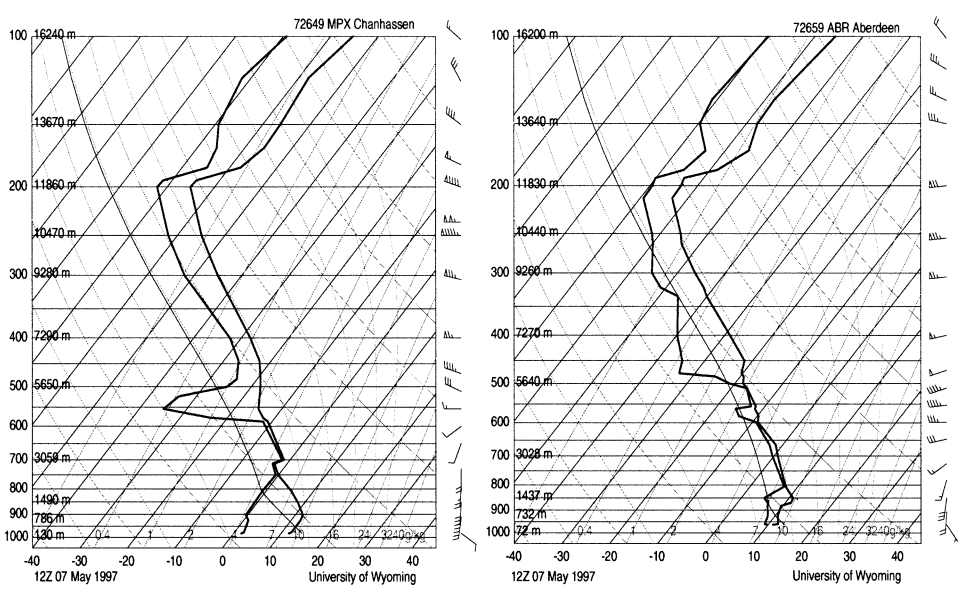

FIG. 3. The 1200 UTC soundings from (a) MPX and (b) ABR, on 7 May 1997.

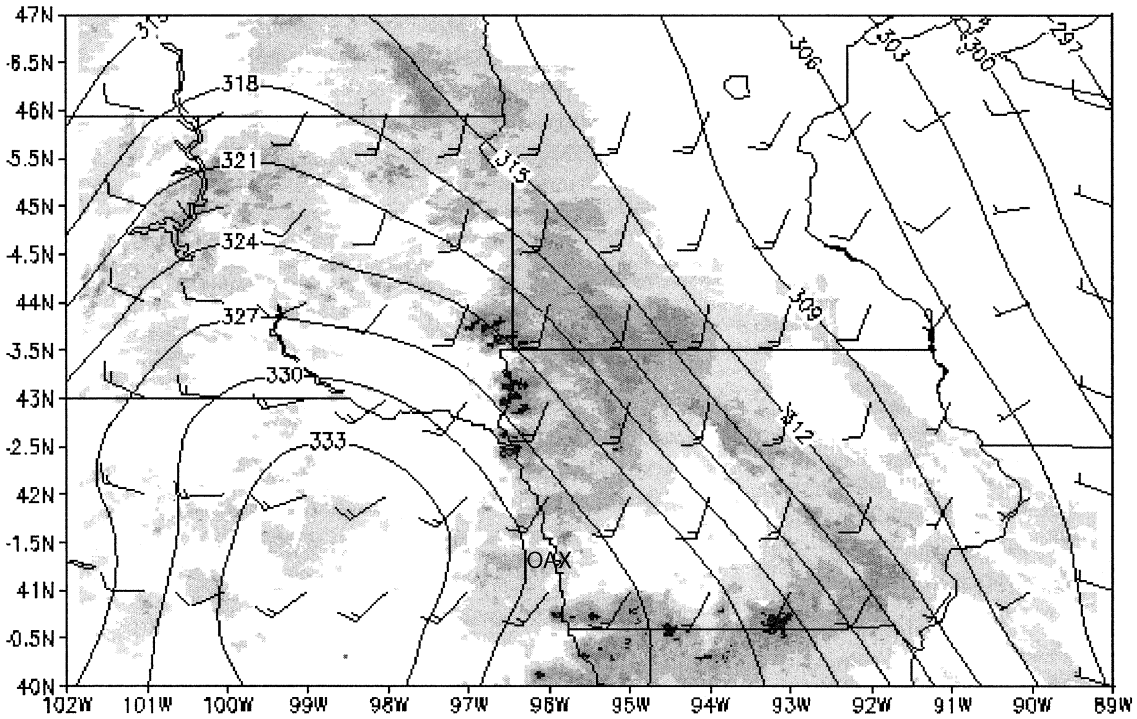

FIG. 4. The 800-hPa analysis of RUC θ_e (contoured every 3 K) at 1200 UTC. Radar reflectivity is shaded: light gray = 20–30 dBZ, medium gray = 30–40 dBZ, dark gray = 40–50 dBZ, and black ≥ 50 dBZ. Ground-relative wind barbs are shown. Half barb = 5 m s^{-1}; full barb = 10 m s^{-1}. Sounding location OAX is indicated.

1990; Trier and Parsons 1993)—on going at this time in northwestern Iowa and adjacent southeastern South Dakota and southwestern Minnesota (Fig. 5), northeast of the surface warm front.

Low-level buoyant air behind the system can be seen in Fig. 4, an 800-hPa analysis of 60-km RUC equivalent potential temperature (θ_e) at 1200 UTC. A θ_e maximum exceeding 333 K was indicated by the RUC analysis west of (behind) the MCS, consistent with the sounding data (OAX measured 333.9 K at 850 mb). Southwesterly flow indicated by this analysis seems to suggest advection of this higher-θ_e air into the rear of the convective line. However, subtracting the observed storm motion (15 m s^{-1} from 262°) from the RUC analysis wind field yields storm-relative winds within the θ_e maximum directed to the northwest—away from the convective line. Nonetheless, radial velocity data from the Sioux Falls, South Dakota, WSR-88D did indeed reveal storm-relative flow toward the MCS, which not only confirms the advection of higher-θ_e air into the rear of the convective line, but also implies that the RUC analysis was unable to accurately resolve the wind field in the vicinity of the MCS.

2) HORIZONTAL REFLECTIVITY STRUCTURE AND SYSTEM EVOLUTION

A sequence of radar reflectivity mosaic data is presented in Fig. 5. The first few convective cells in the developing LS MCS were visible at 0600 UTC (Fig. 5a) in the southeastern corner of South Dakota. They formed along a NW–SE line until 0800 UTC (not shown), when a more N–S orientation began to develop. A stratiform region expanded rapidly after 0700 UTC and continued to expand at 0900 UTC (Fig. 5b). A region of enhanced stratiform precipitation formed well ahead of the convective line at 1200 UTC (Fig. 5c). This enhanced stratiform region continued throughout the storm's lifetime, separated from the convective line by a region of lower reflectivity—a transition zone similar to those seen in TS systems (Smull and Houze 1985). The convective line orientation shifted to NNW–SSE at 1300 UTC (not shown). At 1500 UTC (Fig. 5d), the convective line reorganized into one large convective cell. The line reformed by 1600 UTC (not shown). After 1800 UTC (Fig. 5e) the system became more disorganized and moved out of the area by 2100 UTC (Fig. 5f).

The convective cells within this MCS (and others observed by the authors) were more discontinuous than those typically seen in TS systems (Carbone 1982; Rutledge et al. 1988; Houze et al. 1989, 1990). Some cells were elongated perpendicular to the line (1000 UTC, not shown), while others were elongated at an angle slightly off perpendicular (Fig. 5c). This orientation is similar to the canted alignment of cells of TS systems found by Houze et al. (1990). The elongation of cells perpendicular or slightly canted to the convective line

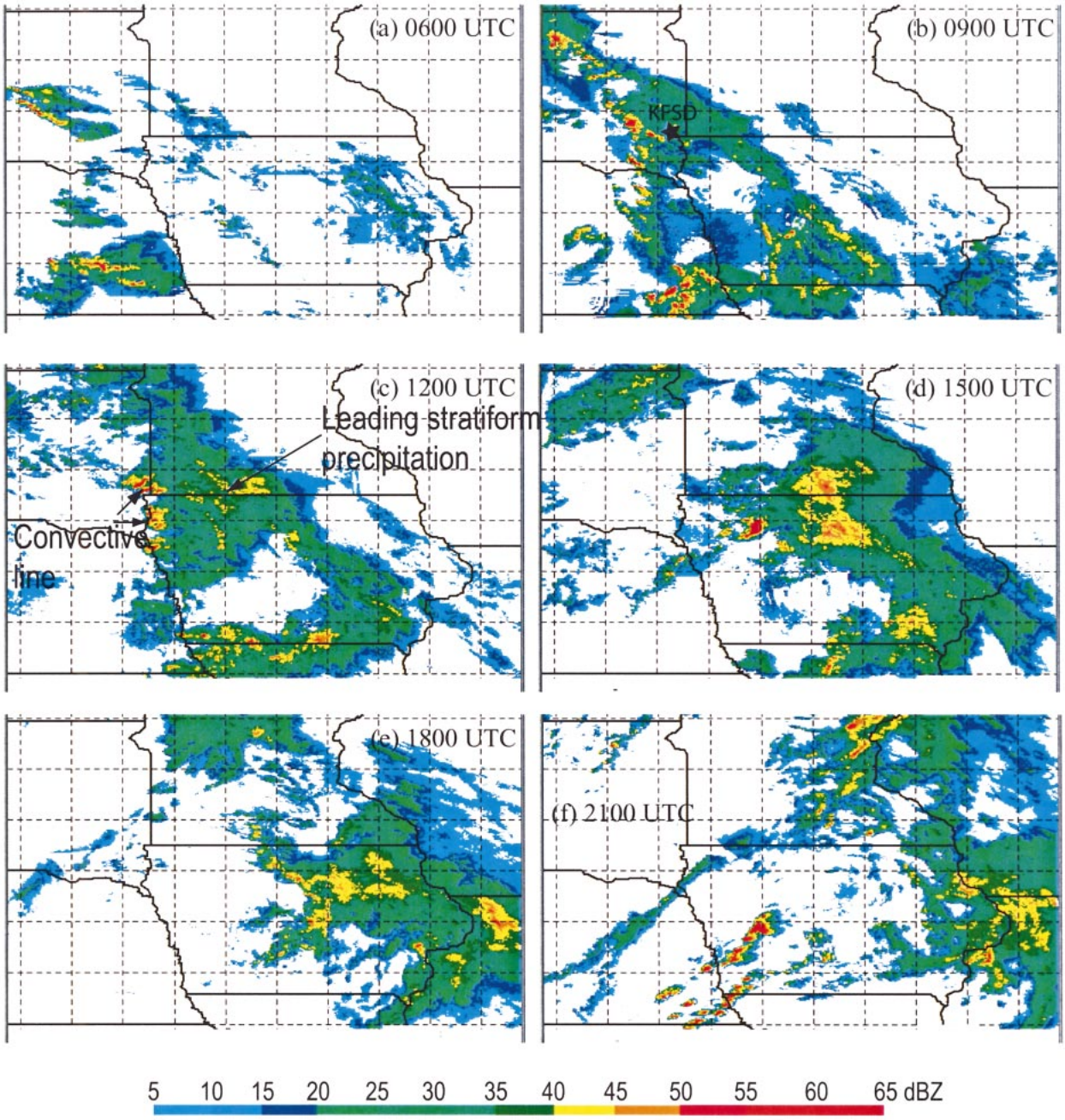

FIG. 5. Radar reflectivity for (a) 0600–(f) 2100 UTC for 7 May 1997.

has been documented behind gust fronts by Weckwerth and Wakimoto (1992) and behind warm fronts by Chapman and Browning (1998) and Wakimoto and Bosart (2001). They attribute the alignment and spacing of the cells to Kelvin–Helmholtz billows that develop in the vertically sheared flow behind the front with the shear vector quasi-parallel to the surface frontal boundary.

The visible satellite image at 1415 UTC provides another view of the system structure (Fig. 6). The satellite image shows the convective cells on the western edge of the system. In addition, there is evidence of lines of developing cells farther to the west, further supporting the idea that the air feeding the convective line is from the rear of the system. If the precipitating cells in the convective line have their origins in these cloud lines, then their orientation and spacing may be ultimately linked to boundary layer instabilities such as horizontal convective rolls, which are known to generate cloud lines approximately aligned with the low-level wind shear (LeMone 1973) and have been observed to pro-

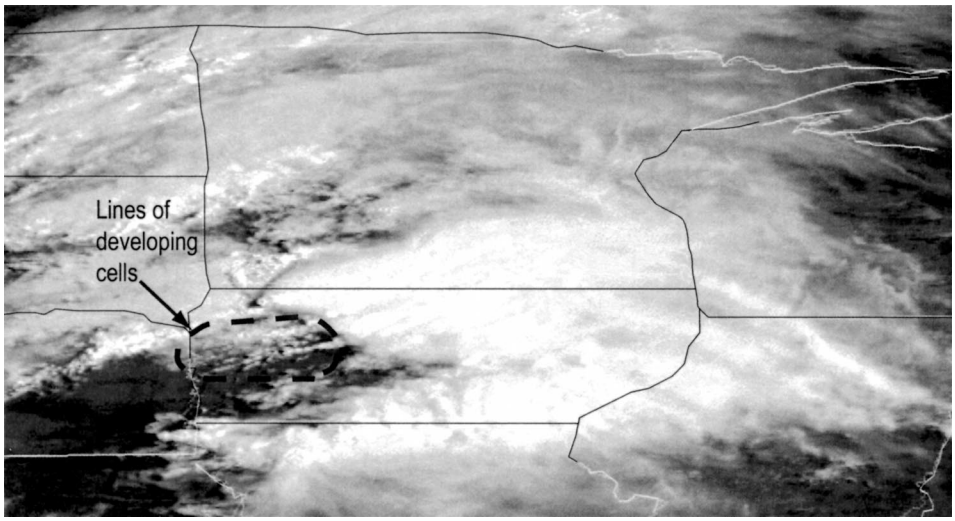

FIG. 6. Visible satellite image over northern Midwest at 1415 UTC on 7 May 1997.

duce lines of deep convection (Trier et al. 1991). A cirrus cloud shield extends downstream (east) of the convection, consistent with the LS structure of the MCS.

3) VERTICAL STRUCTURE

Doppler radar data from the WSR-88D in Sioux Falls, South Dakota (location shown in Fig. 5b), were available to assess vertical structure. An analysis of this dataset provides the vertical structure of the MCS at a much higher resolution than that provided by the other analysis fields. Unfortunately, 3 h of data, from 0742 to 1031 UTC, were missing from the dataset. Prior to 0700 UTC little stratiform rain had developed, and the MCS was far from the radar site. After around 1300 UTC most of the system (especially its stratiform elements) was out of the range of the radar. With these constraints, four vertical cross sections (Figs. 7a–d) were taken along the direction of motion to show the evolution of the system. Cross sections were averaged over a 10-min period (three scans) to reduce noise. Radial velocities are storm relative, with a storm motion vector of 15 m s^{-1} from 262° used to determine storm-relative flow.

At 0733 UTC the system was beginning to produce stratiform rain (Fig. 7a) with front-to-rear (FTR) flow at low levels and rear-to-front (RTF) flow at mid to upper levels (Fig. 7a). Flow behind the system at low to midlevels was indeterminable because of the lack of scatterers in that region and distance from radar. At 1036 UTC the convective line was directly over the radar (Fig. 7b). Ascending RTF flow was seen atop FTR flow. By 1036 UTC, elevated rear inflow can be seen as low as 2 km above ground level (AGL), representing the flow atop the inversion (Fig. 3b). This elevated inflow advected higher θ_e from the west toward the rear of the convective line (Fig. 4). A large leading stratiform precipitation region was developing at this time.

At 1126 UTC the convection had moved east of the radar (Fig. 7c). An elevated rear inflow was evident at about the same height and position relative to the convective line as at 1036 UTC. The FTR flow below 5 km in the analysis domain was now descending (downward sloping), with ascending (upward sloping) RTF flow above it. An enhanced stratiform region had formed, and a transition zone (Smull and Houze 1985) of lower reflectivity centered around 40 km away separated it from the convective line. At 1226 UTC a descending FTR inflow extended to near the surface topped by an ascending RTF flow carrying hydrometeors ahead of the convective line (Fig. 7d). An elevated rear inflow can be seen around 3 km AGL. Apart from the elevated rear inflow feeding the convective line and the absence of a reversal in the descending FTR flow, these circulation features are the mirror image of the FTR flow and rear-inflow jet in a TS system (Houze et al. 1989). More will be said about this comparison later.

These vertical cross sections of radial velocities were compared to the RUC analyses for the same area. The RUC analyses of the wind field for this case, owing to the sparsity of sounding and wind profiler data, were unable to resolve the circulation features within and in the vicinity of the MCS, even in an approximate sense. Moreover, the RUC did not realistically simulate the life cycle of the MCS.

Vertical cross sections were taken of ungridded radar reflectivity to get a sharper picture of the reflectivity structure since gridding tends to spread out smaller-scale features. Cross sections showed a significant bright band (Houze et al. 1989) progressing ahead of the convective line with a transition zone of low reflectivity dividing the two areas (Fig. 8). They also showed evidence of a small trailing anvil (Fig. 8b), similar to the leading anvil seen in a TS system (Fig. 1 of Houze et al. 1989).

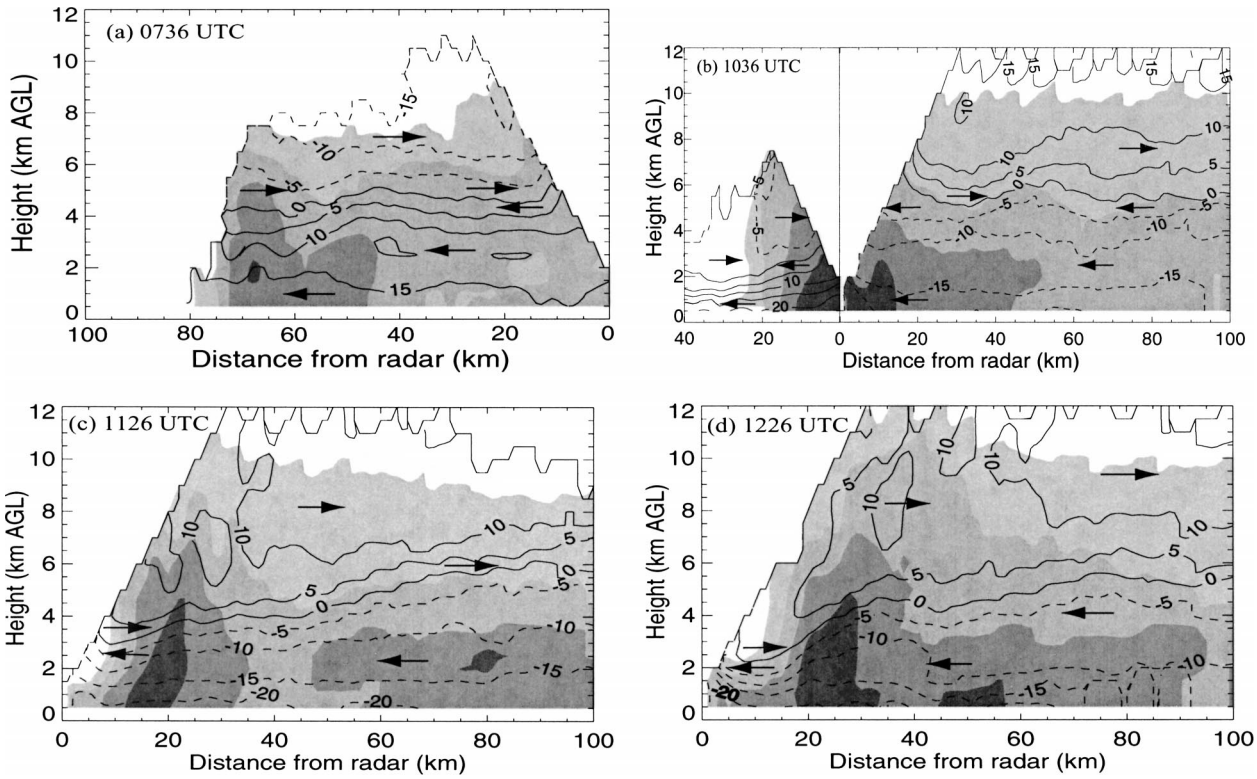

FIG. 7. Average vertical cross section of radar reflectivity and storm-relative flow (m s^{-1}) at (a) 0736, (b) 1036, (c) 1126, and (d) 1226 UTC on 7 May 1997. Radar reflectivity is shaded: light gray = 10–20 dBZ, medium gray = 20–40 dBZ, and black = 40–50 dBZ. Storm-relative flow is contoured every 5 m s^{-1}. Solid contours are away from the radar; dashed contours are toward the radar. Fall speed effects were not factored out; therefore, the analysis of horizontal winds at high-elevation angles is not reliable.

b. LS MCS on 30 April 2000

Unlike the 7 May 1997 case, single-site Doppler radar data were unavailable for the MCS on 30 April 2000. However, other valuable data were available (e.g., surface mesonet and a dense wind profiler network). These additional data permit an investigation of other aspects of the 30 April case that can be compared to the 7 May case to examine similarities and differences between the two events.

1) SYNOPTIC ENVIRONMENT

At 1200 UTC on 30 April 2000, the upper-level flow pattern across the United States featured a short-wave trough and cutoff low embedded within a large-scale ridge over the Rocky Mountains (Fig. 9). The cutoff low was approaching the southern plains, where the LS MCS developed.

A surface low at 1200 UTC was located in the southwestern portion of the Texas Panhandle (Fig. 10). A stationary front stretched slightly northward from the low and then extended southeastward, finally paralleling the Oklahoma–Texas border. The convective line of the MCS was parallel to the stationary front and a stratiform rain region was developing ahead of the convective line. A dryline extended south of the low. A cold front from Nebraska dipped south-southwestward to just north of the low. An outflow boundary from convection north of the LS MCS extended from the Oklahoma panhandle northeastward.

Soundings from Amarillo, Texas (AMA), and Norman, Oklahoma (OUN, locations denoted in Fig. 10), depict the environment behind and ahead of the MCS, respectively (Fig. 11). Amarillo had a moist lower layer, a capping inversion between 700 and 750 hPa, and strong southwesterly flow from the surface up to 300 hPa.

The sounding at OUN ahead of the MCS shows some significant differences. There was a strong temperature inversion near the surface and a moist, stable layer above extending to 800 hPa, reflecting the presence of the stationary front. Winds from the surface up to 300 hPa were much weaker than at AMA and generally veered with height from southeasterly at low levels to southwesterly at midlevels. Above 300 hPa the flow was stronger and nearly saturated, reflecting the cirrus outflow from the MCS near the Oklahoma–Texas border.

2) HORIZONTAL CLOUD AND PRECIPITATION STRUCTURE AND THEIR EVOLUTION

A sequence of 3-hourly reflectivity maps shows the evolution of the MCS from 0600 to 1800 UTC on 30

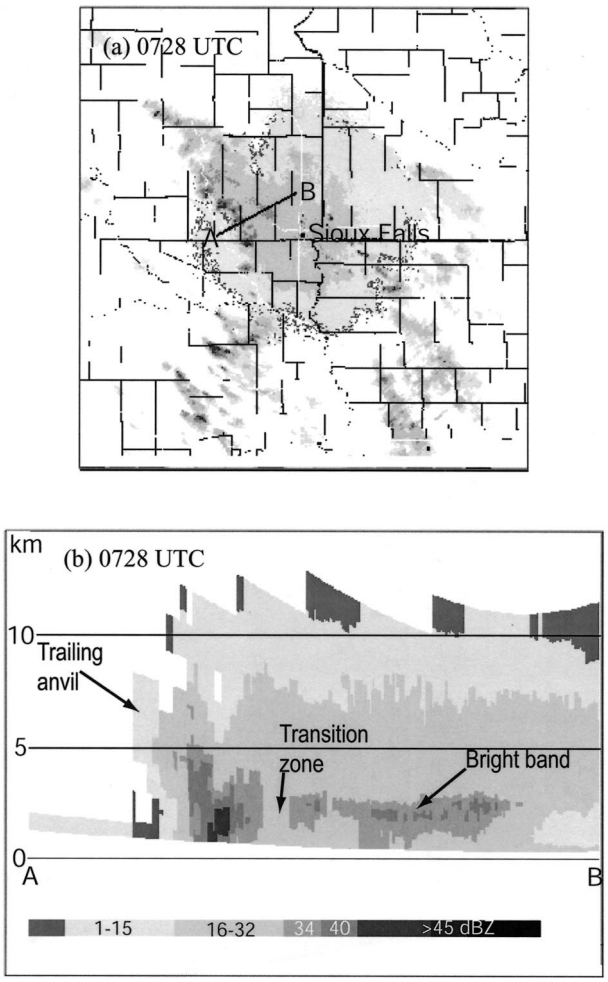

FIG. 8. (a) Radar reflectivity at 0728 UTC from Sioux Falls, SD, WSR-88D. Line A–B is used for (b). (b) Vertical cross section of ungridded radar reflectivity at 0728 UTC taken along the line A–B in (a).

April (Fig. 12). From 0600 to 1200 UTC the convective line of the LS MCS developed along a NW–SE line just west of the Oklahoma–Texas border, but there was little overall system motion. Leading stratiform rain began to develop between 0600 and 0900 UTC (Figs. 12a and 12b). It expanded toward the northeast and developed all along the convective line by 1200 UTC (Fig. 12c). By 1400 UTC (not shown), a transition zone developed between the stratiform rain and the convective line, similar to the 7 May case. The stratiform rain continued to expand to the northeast through 1500 UTC (Fig. 12d), but the overall area contracted after that. The stratiform rain led the convective cells until 1800 UTC (Fig. 12e).

The slow system motion early in the life cycle contributed to the heavy rains that occurred over southwestern Oklahoma. Over 100 mm of rain fell in central and southwest Oklahoma, causing flooding in these areas (Fig. 13). Animations of radar reflectivity show evidence of back-building cells, which then moved over the same area producing heavy rain (Bluestein and Jain 1985; Chappell 1986) and also contributed to the floods of the day.

The convective cells of the MCS were very discontinuous. Early in the system's lifetime they were elongated approximately perpendicular to the convective line (Fig. 12c). As the system matured (Fig. 12d), convective cells appeared canted at 45°–60° angles with respect to the line. This latter pattern is similar to the 7 May case, and also to TS MCSs (Houze et al. 1990).

The visible satellite image at 1415 UTC (Fig. 14) confirms what the radar data imply. Strong convective cells are seen at the western edge of the system, which is consistent with the location of the high radar reflectivities around that time (Fig. 12d). As in the 7 May 1997 case, lines of cumulus clouds can be seen extending southwest of the convective line. There is a distinctive difference between cloud tops at the southwestern edge of the MCS and those to the northeast. The cloud top is more uniform to the northeast, consistent with stratiform rain in this area. The overall appearance of this LS MCS in the visible satellite imagery closely resembled that for the 7 May 1997 case (Fig. 6).

3) SURFACE FEATURES

A mesolow that formed ahead of the stratiform rain region is apparent in the mesonet data. A station plot displaying the effect of this mesolow at station MANG in the Oklahoma Mesonet (position indicated in Fig. 12a) is shown in Fig. 15. A similar pattern was seen at 13 other sites. The stratiform rain for this station began 75 min after the passage of the mesolow, with convective rain not arriving for another few hours. In a general sense, the time series in Fig. 15 is the reverse of that for a TS system, where the wake low appears at the back edge of the stratiform rain region (Johnson and Hamilton 1988, their Fig. 11). However, the analogy between the two systems (LS and TS) is not obvious. Unlike the wake low associated with a TS MCS, which has been observed to move with the stratiform region (according to Johnson and Hamilton 1988), this mesolow stayed ahead of the stratiform rain and moved to the southeast at 11 m s^{-1} (not shown), and was later replaced by another leading mesolow. Further analyses were performed to determine if the mesolow had gravity-wave-like structure as has been done by Koch and Siedlarz (1999), and indeed a gravity wave signature was found at several sites; however, an evaluation of the nature of its origin proved inconclusive. Haertel and Johnson (2000) found a leading mesohigh–trailing wake low couplet in association with a propagating low-level cool source due to stratiform precipitation evaporation; however, the mesolow in this case occurred ahead of the stratiform region and at a time when the stratiform region was more-or-less stationary (although it was expanding), so the mechanism of Haertel and Johnson

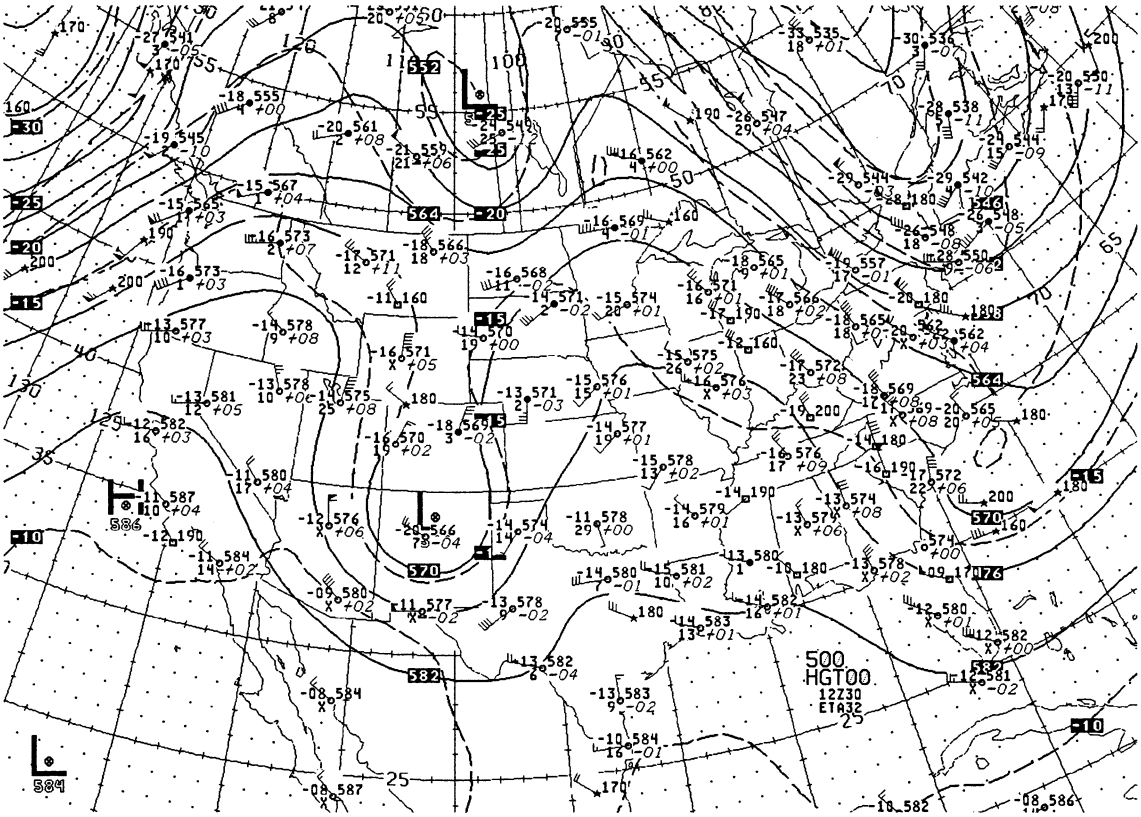

FIG. 9. NCEP 500-hPa analysis chart for 1200 UTC on 30 Apr 2000: heights (dm, solid contours) and temperatures (°C, dashed contours).

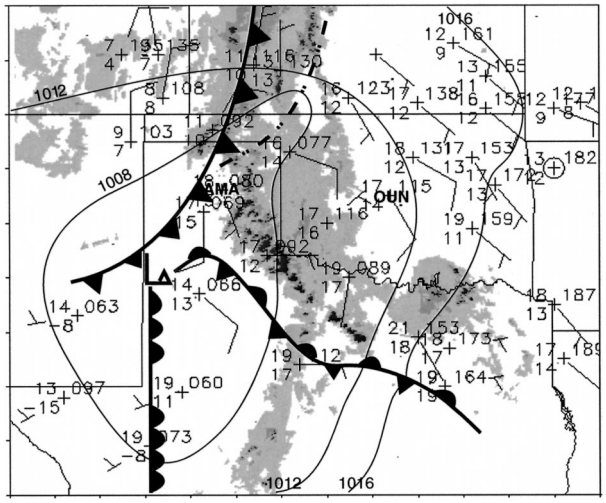

FIG. 10. Surface analysis for 1200 UTC on 30 Apr 2000. Radar reflectivity is shaded as in Fig. 2. Pressure is contoured every 4 hPa. Scalloped curve denotes a dryline and dash–double dot curve denotes an outflow boundary. Locations of sounding sites AMA and OUN are indicated.

(2000) does not appear to be the explanation for the mesolow.

Several sites in the Oklahoma Mesonet revealed heat bursts (Johnson 1983; Johnson et al. 1989) associated with the leading mesolow. The station plot for CHEY (position indicated in Fig. 12a) shows evidence of a strong heat burst around 1130 UTC (Fig. 16) just prior to the start of stratiform rain (not shown). From 1045 to 1125 UTC, the temperature rose 5.5°C, and the relative humidity fell 44%. Station pressure reached a minimum at 1120 UTC, having fallen 1.6 hPa. Similar surface changes due to heat bursts were reported by Johnson et al. (1989). Winds shifted from west-southwesterly to easterly and increased in speed from 5 to 9 m s^{-1} (not shown). Similar, weaker features are seen at several stations. Analyzing the time and location of these heat bursts places them just ahead of the stratiform rain as seen by radar. This location supplies an explanation for a possible mechanism for the heat bursts. As air beneath the stratiform anvil is evaporatively cooled it becomes cooler than the surrounding air and sinks. As it sinks it is warmed by compression, and if the lower troposphere is nearly dry adiabatic, the sinking air can gain enough momentum to break through the stable layer and reach the surface as a heat burst (Johnson 2001). This particular case appears to correspond well with the lateral

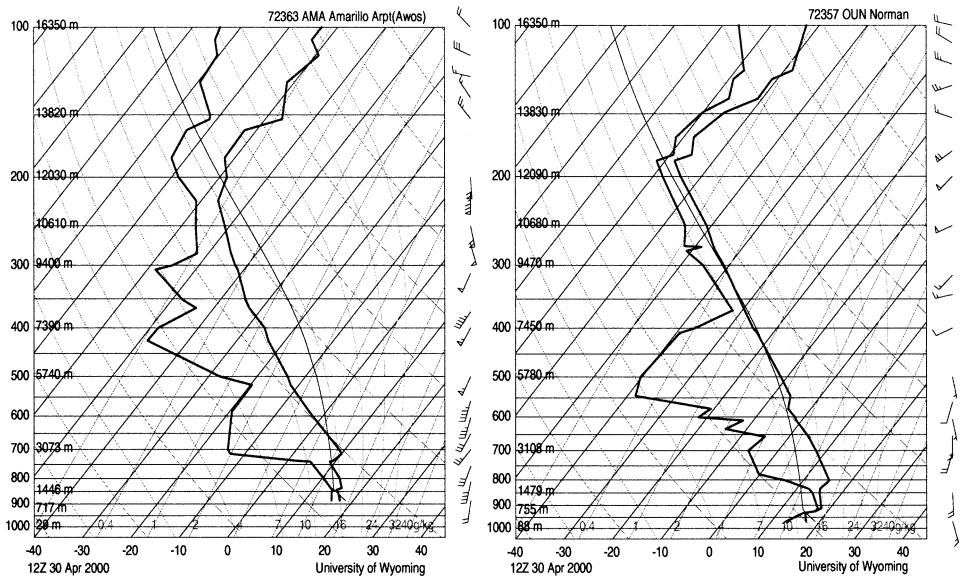

(a) Amarillo, Texas (b) Norman, Oklahoma

FIG. 11. The 1200 UTC soundings from (a) AMA and (b) OUN on 30 Apr 2000.

inflow jet described by Bernstein and Johnson (1994). Although the heat bursts do not seem to progress in any one direction, they appear to correspond approximately with the location of the leading low. Eight of the 11 heat bursts occurred between 1100 and 1200 UTC. The heat bursts in this region provide strong evidence of sinking motion within the stratiform precipitation area.

4) VERTICAL STRUCTURE

Since single-site Doppler radar data were unavailable for the 30 April LS MCS, wind profiler network data, as well as 40-km RUC analyses, were used to construct the vertical profile of the environmental flow. Although it is recognized that these data cannot describe the internal circulations of the system, the positioning of the system in proximity to the densest part of the NPN network offers hope that the circulation in the environment of the system is reasonably well sampled.

A vertical cross section of θ_e (along line A–B in Fig. 12d) from the 40-km RUC at 1500 UTC can be seen in Fig. 17.[2] An axis of high-θ_e air can be seen between 850 and 800 hPa in the western part of the cross section (behind the convective line). Although the RUC does not resolve the flow within the system, it does indicate an elevated rear inflow of high-θ_e air, as in Colman (1990), Trier and Parsons (1993), and Smull and Augustine (1993). The RUC also suggests a θ_e maximum at 850 hPa, collocated with the stratiform precipitation at this time. A stable layer can be seen from the surface up to this θ_e maximum.

A vertical cross section of the convective line-normal wind component of the storm-relative flow along line A–B in Fig. 12d at 1500 UTC is shown in Fig. 18. This cross section is based on an objective analysis of winds from the profiler network, but with winds calculated in a storm-relative framework, using a storm motion vector of 9 m s^{-1} from 212° (this storm motion vector was also used for Fig. 17). An extensive stratiform region had developed by 1500 UTC, making it more likely that the profiler network resolved some of the large-scale features of the LS MCS.

This cross section, similar to the RUC cross section in Fig. 17, suggests an elevated RTF feed of high-θ_e air into the rear of the convective line. This analysis also suggests an RTF flow of air in the upper troposphere, which ascends in the region over, and just upstream of, the MCS, and then descends ahead of the stratiform rain region. Also indicated ahead of the stratiform rain is a storm-relative current flowing FTR at midlevels, generally above 4 km. There is some evidence of descent within this air stream east of 96°W above approximately 6 km. This FTR, slightly descending air stream may be evidence of a ''leading inflow jet,'' analogous, from an observational perspective, to the rear-inflow jet in a TS MCS. Assuming that this inflow jet indeed descends to low levels (not shown in the coarse data analyses used in this study), this jet may be the mechanism responsible for the observed heat bursts, in a manner similar to that described in Bernstein and Johnson (1994) and Johnson (2001). Finally, the profiler data indicate a layer of RTF

[2] A portion of the lower part of the analyses in Figs. 17 and 19 has been extrapolated to below ground.

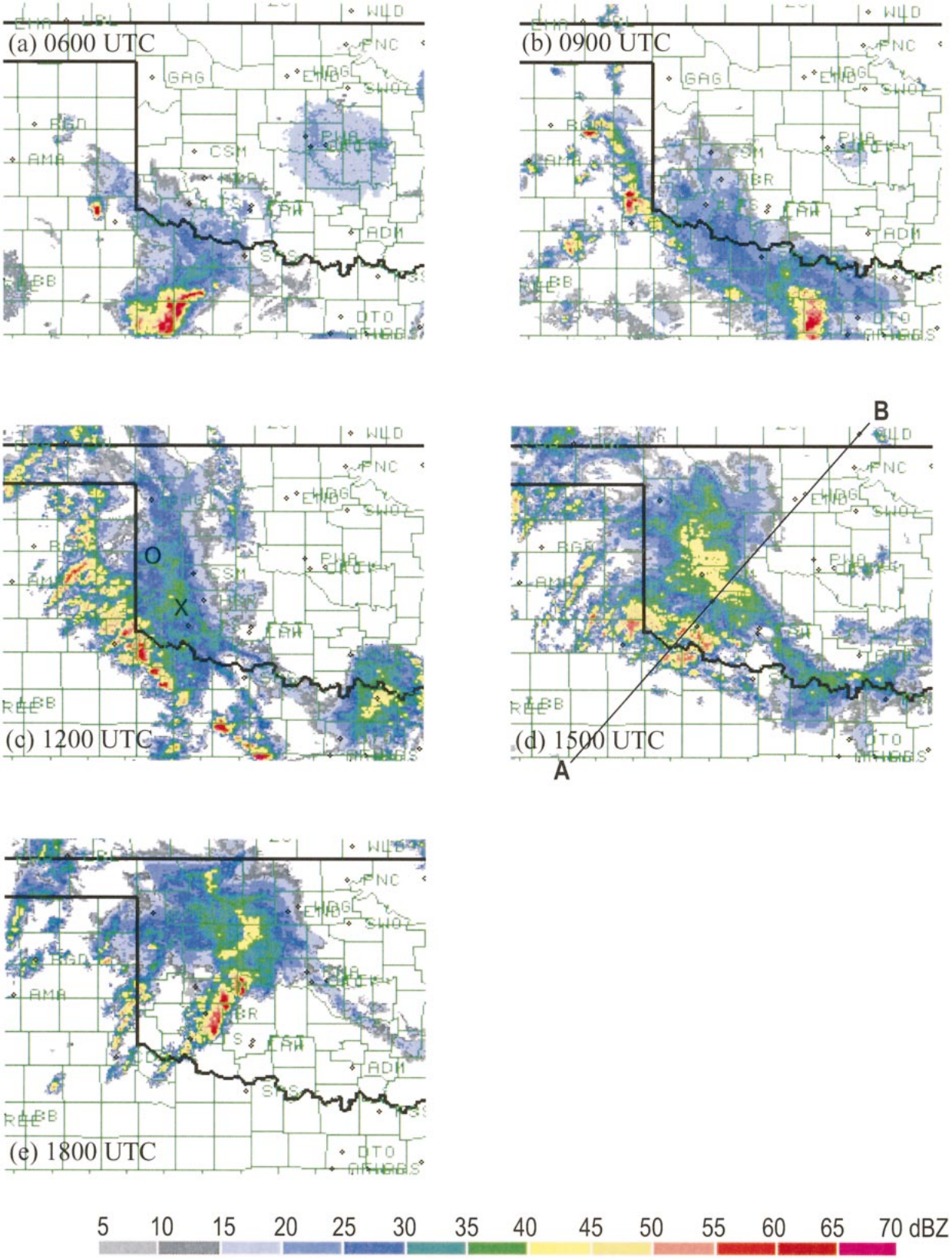

FIG. 12. Three-hourly time series of radar reflectivity for 30 Apr 2000. In (c), location of mesonet station MANG is indicated by X and CHEY by O. In (d), line A–B is shown and to be used for Figs. 17–19.

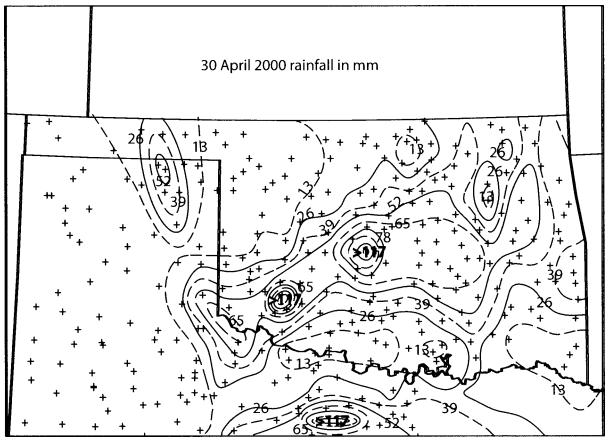

FIG. 13. Total rainfall (in mm) gathered from 313 cooperative stations for 30 Apr 2000. Station locations are indicated by +. Two maxima (>117+) in OK were the locations of flash floods.

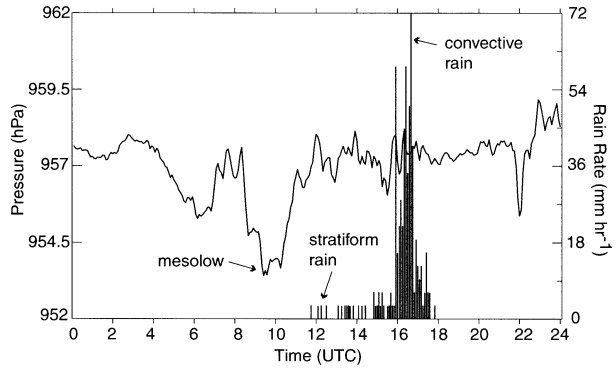

FIG. 15. Station plot for MANG in the OK Mesonet (see Fig. 12a for location) on 30 Apr 2000. Pressure (line) is in hPa, rain rate (vertical bars) in mm h^{-1} based on 5-min observations.

flow throughout the domain at low levels (generally below 2 km).

Most of the features seen in the profiler data for the 30 April case are consistent with the radar cross sections for the 7 May case; however, there was no RTF flow at low levels seen in the radar data for 7 May (Fig. 7). Considering the coarse resolution of the profiler data (Xs at the top of Fig. 18), the low-level RTF flow may be an artifact of the low-resolution profiler data. While large-scale features are resolved, certain small-scale features, such as the low-level divergent flow near 97°W in Fig. 18, are considered unreliable.

A cross section of potential temperature, relative humidity, and storm-relative wind can be seen in Fig. 19. Evidence of the stationary front is visible on the west side of the cross section centered near 800 hPa. The position of this front is farther west in Fig. 19 than it is in Fig. 10; however, this discrepancy may be due to the resolution of the RUC. A cold pool of <294 K that may be connected with the MCS is seen in Fig. 19. Isentropic surfaces slant upward from west to east from 850 to 500 hPa, indicating frontal lifting could have played an important role in the generation of convection (e.g., Colman 1990; Trier and Parsons 1993) and could also have enhanced precipitation in the stratiform region.

In summary, vertical cross sections of gridded wind profiler data depict the vertical flow structure of the 30 April 2000 LS MCS to resemble in a broad sense the circulation associated with the 7 May 1997 LS MCS. The midlevel, descending FTR flow ahead of the convective line is to a good approximation the mirror image of a TS system rear-inflow jet. However, not all aspects of the flow are a mirror image. An elevated rear inflow exists that feeds the system high-θ_e air from behind. The TS systems are fed at the leading edge from air rooted in the boundary layer. The slightly elevated RTF flow feeding the convective line in these LS systems is different than depicted in Parker and Johnson (2000, their Fig. 12), which shows FTR storm-relative flow at this level based on average soundings ahead of the system. However, Parker and Johnson (2000) provided evidence that indeed some of the LS systems they studied were fed from the rear. An ascending RTF flow aloft carries hydrometeors ahead of the convective line to form the

FIG. 14. Visible satellite image centered over OK at 1415 UTC on 30 Apr 2000.

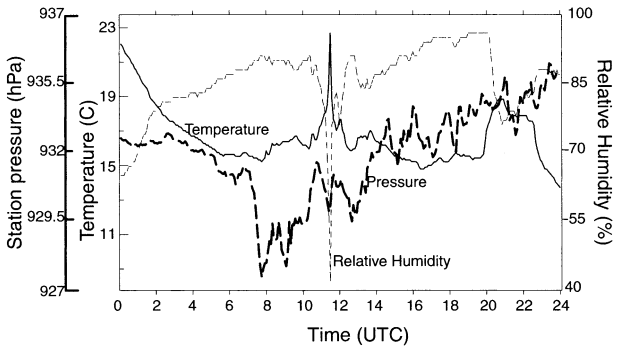

FIG. 16. Station plot for CHEY in the OK Mesonet (see Fig. 12a for location). Temperature (solid line) is in °C. Pressure (thick dashed line) is in hPa. Relative humidity (thin dashed line) is in %.

stratiform region there, consistent with the Parker and Johnson (2000) model. Isentropic upglide introduces the potential for frontal lifting to initiate or prolong convection or enhance the stratiform region. A sharp frontal inversion caused by the quasi-stationary front decouples the surface flow (which was FTR throughout) from the elevated rear inflow.

4. Summary and conclusions

Various datasets—including single-site and national mosaic Doppler radar, NOAA Wind Profiler Network, RAOBs, the Oklahoma Mesonet, and the 40-km and 60-km RUC model, were combined to analyze the airflow and precipitation features of two leading stratiform (LS) mesoscale convective systems (MCSs). A schematic diagram of the common airflow and precipitation features of these two MCSs is contained in Fig. 20. In addition, the main findings that resulted from the study are summarized as follows:

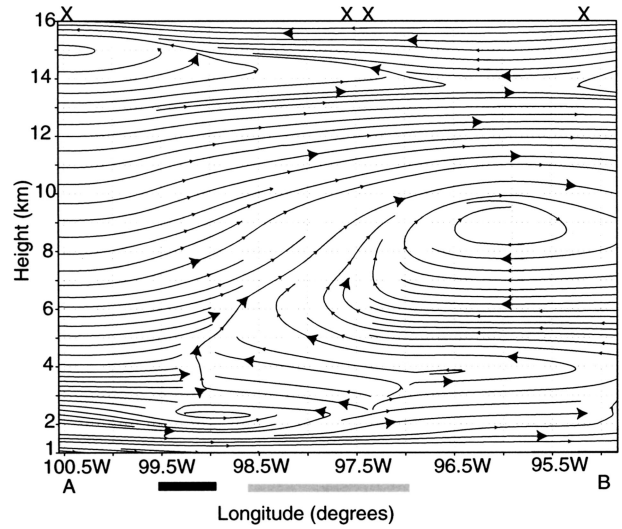

FIG. 18. Vertical cross section of profiler-derived storm-relative streamlines along A–B in Fig. 12d for 1500 UTC. Black bar indicates convective region; gray bar indicates stratiform region. The Xs indicate profilers' closest point of approach to the cross section.

- Overall airflow (based on vertical cross sections of radar radial velocity in the 7 May 1997 case, and of gridded data from four NOAA wind profilers in the 30 April 2000 case) appeared to be very similar for both cases. The airflow consisted of three main branches: 1) an elevated, rear inflow at 2–3 km, which transported high-θ_e air into the convective line (lines that, in both cases, were elevated, having developed above a surface stable layer on the cool side of a warm/stationary boundary); 2) an ascending rear-to-front (RTF) flow at upper levels that carried hydrometeors downstream from the convective line, thus resulting in the leading stratiform/anvil region [consistent with

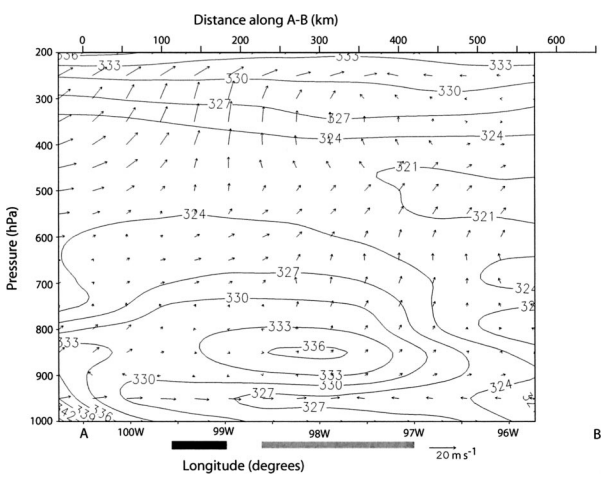

FIG. 17. Vertical cross section of RUC equivalent potential temperature (θ_e, K) and storm-relative wind vectors (vertical motion has been multiplied by 100) at 1500 UTC along the line A–B in Fig. 12d. Black bar indicates convective region; gray bar indicates stratiform region.

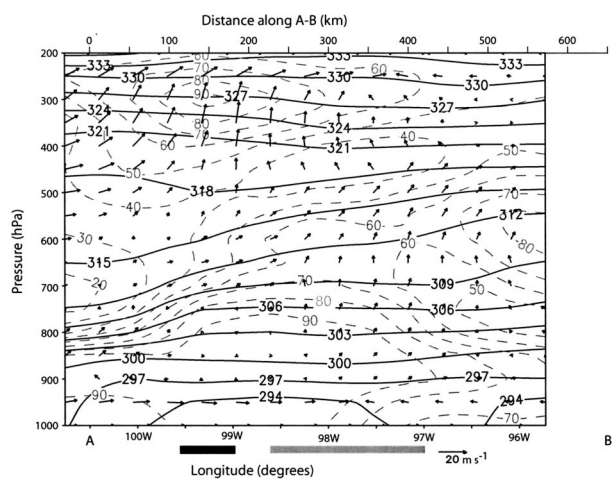

FIG. 19. Vertical cross section of RUC potential temperature (θ, K, black contours), relative humidity in % (dashed gray contours), and storm-relative wind vectors (vertical motion has been multiplied by 100) at 1500 UTC 30 Apr 2000 along line A–B in Fig. 12d. Black bar indicates convective region; gray bar indicates stratiform region.

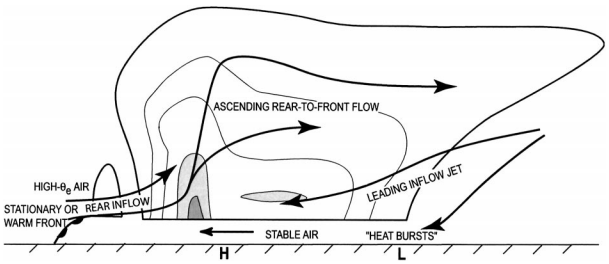

FIG. 20. Conceptual model of a rear-fed LS MCS above a stable surface layer viewed in a vertical cross section oriented perpendicular to the convective line (i.e., parallel to its motion) during the mature stage of its life cycle. Arrows indicate mean, storm-relative flow. Radar reflectivity is indicated by thin contours. Cloud outline is thicker contour. Areas of enhanced reflectivity are shaded. Surface high and low pressure centers are indicated by H and L, respectively.

the Parker and Johnson (2000) model]; and 3) a descending front-to-rear (FTR) flow (beneath the leading anvil) at low to midlevels, herein termed the leading inflow jet.

- In many respects, the precipitation and airflow features associated with the two LS systems analyzed in this study observationally resemble (in a ''reversed,'' or ''mirror image'' sense) those found in trailing stratiform (TS) systems (Houze et al. 1989). For instance, the convective line in these two MCSs was separated from an enhanced, or higher, radar reflectivity stratiform precipitation region by a region of lower reflectivity, as has been observed in TS systems. Also, the ascending RTF flow at upper (anvil) levels (mentioned earlier) identified in this study resembles the ascending FTR flow found in TS systems. Likewise, the descending rear-inflow jet associated with TS MCSs. However, in some respects, the airflow observed within these two LS MCSs differs from that identified with TS systems. For example, the leading inflow jet in these two cases did not appear to reverse direction at low levels near the convective line, as does the rear-inflow jet in TS systems. Moreover, the elevated rear inflow observed with these two LS systems differs from the boundary layer inflow into the front of the convective line associated with the TS systems. [It should be noted here that although the two LS MCSs in this study were elevated (cold sector) and rear-fed, Parker and Johnson (2000) identified several warm-sector LS MCSs that appeared to be front-fed. Therefore, the conceptual model presented here (particularly in terms of the flow observed at low levels) is likely unrepresentative of some LS MCSs.] Another difference noted between the two LS MCSs in this study and TS systems was the observation that the convective line in both of these cases was discontinuous in terms of individual cell spacing, whereas the convective line is generally more ''solid'' or continuous in TS systems. Finally, although data for the 30 April 2000 case in this study did reveal a mesolow just ahead of the stratiform rain region, similar to the location of the wake low in a typical TS system, the movement of the low in this case differed from that of a mesolow in a TS system—as it moved paralled to the stratiform rain region and eventually away from the MCS, whereas TS wake lows generally remain along the back of the stratiform rain region throughout the TS system's life cycle.

While this study provides observations of two rear-fed LS MCSs, it should be noted that both cases were sparsely sampled observationally, as the study was based solely on operational datasets. Single-site Doppler radar data were only available for one of the cases (the 7 May 1997 case), which (along with the fact that only two cases were analyzed) suggests a significant amount of uncertainty in terms of generalizing the results, or applying the proposed conceptual model to other LS MCS cases. A study of several additional, more thoroughly observed LS systems would be beneficial to extend the flow characteristics suggested for these two cases to other LS systems. In particular, a dual-Doppler study of several LS systems would provide much better information in terms of vertical motion within these systems, as well as the overall storm-relative flow structure in general.

Further study of these MCSs would also provide additional insight into how these systems are similar to or different from TS systems. Since rear-fed LS systems often are associated with heavy rain/flash flooding [due at least in part to the potential for slow-moving/back-building storms within the main convective line (Chappell 1986)], a study of the environmental conditions favorable for LS MCS development—and particularly elevated/rear-fed LS MCSs—would be useful. Although both LS MCSs in this study were elevated and fed from the rear, Parker and Johnson (2000) showed several LS MCSs that occurred in a warm-sector air mass and were front-fed. Observational and modeling studies may be helpful in order to determine what effect these and other variations on the LS MCS theme might have on the potential for heavy rainfall/flash flooding.

Acknowledgments. The authors would like to acknowledge Andrea Williams, Dr. Rob Cifelli, Paul Ciesielski, and Paul Hein for their help with radar data processing, as well as Dr. Steve Rutledge of Colorado State University and three reviewers for their helpful suggestions. This research was supported by the National Science Foundation under Grants ATM-9618684 and ATM-0071371, as well as by a one-year graduate fellowship from the American Meteorological Society and Silicon Graphics, Inc.

REFERENCES

Barnes, S. L., 1973: Mesoscale objective analysis using weighted time-series observations. NOAA Tech. Memo. ERL NSSL-62, National Severe Storms Laboratory, Norman, OK, 60 pp. [NTIS COM-73-10781.]

Benjamin, S. G., J. M. Brown, K. J. Brundage, B. E. Schwartz, T. G. Smirnova, and T. L. Smith, 1998: The operational RUC-2. Preprints, *16th Conf. on Weather Analysis and Forecasting,* Phoenix, AZ, Amer. Meteor. Soc., 249–252.

Bernstein, B. C., and R. H. Johnson, 1994: A dual-Doppler radar study of an OK PRE-STORM heat burst event. *Mon. Wea. Rev.,* **122,** 259–273.

Bluestein, H. B., and M. H. Jain, 1985: Formation of mesoscale lines of precipitation: Severe squall lines in Oklahoma during the spring. *J. Atmos. Sci.,* **42,** 1711–1732.

Brock, F. V., K. C. Crawford, R. L. Elliott, G. W. Cuperus, S. J. Stadler, H. L. Johnson, and M. D. Eilts, 1995: The Oklahoma Mesonet: A technical overview. *J. Atmos. Oceanic Technol.,* **12,** 5–19.

Carbone, R. E., 1982: A severe frontal rainband. Part I: Stormwide hydrodynamic structure. *J. Atmos. Sci.,* **39,** 258–279.

Chapman, D., and K. A. Browning, 1998: Use of wind-shear displays for Doppler radar data. *Bull. Amer. Meteor. Soc.,* **79,** 2685–2692.

Chappell, C. F., 1986: Quasi-stationary convective events. *Mesoscale Meteorology and Forecasting,* P. S. Ray, Ed., Amer. Meteor. Soc., 289–310.

Colman, B. R., 1990: Thunderstorms above frontal surfaces in environments without positive CAPE. Part II: Organization and instability mechanisms. *Mon. Wea. Rev.,* **118,** 1123–1144.

Doswell, C. A., III, H. E. Brooks, and R. A. Maddox, 1996: Flash flood forecasting: An ingredients-based methodology. *Wea. Forecasting,* **11,** 560–581.

Fujita, T. T., 1955: Results of detailed synoptic studies of squall lines. *Tellus,* **7,** 405–436.

Haertel, P. T., and R. H. Johnson, 2000: The linear dynamics of squall-line mesohighs and wake lows. *J. Atmos. Sci.,* **57,** 93–107.

Houze, R. A., Jr., 1977: Structure and dynamics of a tropical squall-line system observed during GATE. *Mon. Wea. Rev.,* **105,** 1540–1567.

——, S. A. Rutledge, M. I. Biggerstaff, and B. F. Smull, 1989: Interpretation of Doppler weather radar displays of midlatitude mesoscale convective systems. *Bull. Amer. Meteor. Soc.,* **70,** 608–619.

——, B. F. Smull, and P. Dodge, 1990: Mesoscale organization of springtime rainstorms in Oklahoma. *Mon. Wea. Rev.,* **118,** 613–654.

Johnson, B. C., 1983: The heat burst of 29 May 1976. *Mon. Wea. Rev.,* **111,** 1776–1792.

Johnson, R. H., 2001: Surface mesohighs and mesolows. *Bull. Amer. Meteor. Soc.,* **82,** 13–31.

——, and P. J. Hamilton, 1988: The relationship of surface pressure features to the precipitation and airflow structure of an intense midlatitude squall line. *Mon. Wea. Rev.,* **116,** 1444–1472.

——, S. Chen, and J. J. Toth, 1989: Circulations associated with a mature-to-decaying midlatitude mesoscale convective system. Part I: Surface features—Heat bursts and mesolow development. *Mon. Wea. Rev.,* **117,** 942–959.

Koch, S. E., and L. M. Siedlarz, 1999: Mesoscale gravity waves and their environment in the central United States during STORM-FEST. *Mon. Wea. Rev.,* **127,** 2854–2879.

——, M. DesJardins, and P. J. Kocin, 1983: An interactive Barnes objective map analysis scheme for use with satellite and conventional data. *J. Appl. Meteor.,* **22,** 1487–1502.

LeMone, M. A., 1973: The structure and dynamics of horizontal roll vortices in the planetary boundary layer. *J. Atmos. Sci.,* **30,** 1077–1091.

Maddox, R. A., and C. A. Doswell, 1982: Examination of jet stream configurations, 500-mb vorticity advection, and low-level thermal advection patterns during extended periods of intense convection. *Mon. Wea. Rev.,* **110,** 184–197.

O'Brien, J. J., 1970: Alternative solutions to the classical vertical velocity problem. *J. Appl. Meteor.,* **9,** 197–203.

Oye, R., and R. E. Carbone, 1981: Interactive Doppler editing software. Preprints, *20th Conf. on Radar Meteorology,* Boston, MA, Amer. Meteor. Soc., 683–689.

Parker, M. D., and R. H. Johnson, 2000: Organizational modes of midlatitude mesoscale convective systems. *Mon. Wea. Rev.,* **128,** 3413–3436.

Pedgley, D. E., 1962: A meso-synoptic analysis of the thunderstorms on 28 August 1958. British Meteorological Office Geophysical Memo. 106, 74 pp.

Rutledge, S. A., R. A. Houze Jr., and M. I. Biggerstaff, 1988: The Oklahoma–Kansas mesoscale convective system of 10–11 June 1985: Precipitation structure and single-Doppler radar analysis. *Mon. Wea. Rev.,* **116,** 1409–1430.

Smull, B. F., and R. A. Houze Jr., 1985: A midlatitude squall line with a trailing stratiform rain: Radar and satellite observations. *Mon. Wea. Rev.,* **113,** 117–133.

——, and J. A. Augustine, 1993: Multiscale analysis of a mature mesoscale convective complex. *Mon. Wea. Rev.,* **121,** 103–132.

Trier, S. B., and D. B. Parsons, 1993: Evolution of environmental conditions preceding the development of a nocturnal mesoscale convective complex. *Mon. Wea. Rev.,* **121,** 1078–1098.

——, D. B. Parsons, and J. H. E. Clark, 1991: Environment and evolution of a cold-frontal mesoscale convective system. *Mon. Wea. Rev.,* **119,** 2429–2455.

Wakimoto, R. M., and B. L. Bosart, 2001: Airborne radar observations of a warm front during FASTEX. *Mon. Wea. Rev.,* **129,** 254–274.

Weckwerth, T. M., and R. M. Wakimoto, 1992: The initiation and organization of convective cells atop a cold-air outflow boundary. *Mon. Wea. Rev.,* **120,** 2169–2187.

Zipser, E. J., 1969: The role of organized unsaturated convective downdrafts in the structure and rapid decay of an equatoril disturbance. *J. Appl. Meteor.,* **8,** 799–814.

——, 1977: Mesoscale and convective-scale downdrafts as distinct components of squall-line circulation. *Mon. Wea. Rev.,* **105,** 1568–1589.